X-650-65-75

THE INFRARED INTERFEROMETER SPECTROMETER EXPERIMENT (IRIS)

(VOLUME II - METEOROLOGICAL MISSION)

MARCH 1965

NASA — GODDARD SPACE FLIGHT CENTER —
GREENBELT, MARYLAND

X-650-65-75

THE INFRARED INTERFEROMETER SPECTROMETER EXPERIMENT (IRIS)

(VOLUME II – METEOROLOGICAL MISSION)

by

R. A. Hanel, Goddard Space Flight Center

and

L. Chaney, University of Michigan

February 1965

Goddard Space Flight Center
Greenbelt, Maryland

THE INFRARED INTERFEROMETER SPECTROMETER EXPERIMENT (IRIS)

(VOLUME II – METEOROLOGICAL MISSION)

by

R. A. Hanel, Goddard Space Flight Center

and

L. Chaney, University of Michigan

ABSTRACT

The goals of the IRIS Experiment are the measurement of parameters describing the vertical structure of the atmosphere such as temperature, humidity and cloud height. This information is extracted from the thermal emission spectrum between 5 and 20 μ. A Michelson type interferometer capable of resolving to 5 cm^{-1} is described in detail.

ACKNOWLEDGMENTS

In addition to the authors, the following people made substantial contributions to the effort presented here:

Fred Bartman, University of Michigan
(Useful discussion on Fourier Spectroscopy)

Lawrence Byrne, Goddard Space Flight Center
(Synthesis and analysis of simulated interferograms)

Grady Nichols, Goddard Space Flight Center
(Design and construction of breadboard electronic circuitry)

CONTENTS

LIST OF ILLUSTRATIONS

TABLE

THE INFRARED INTERFEROMETER SPECTROMETER EXPERIMENT (IRIS)

(VOLUME II - METEOROLOGICAL MISSION)

SUMMARY

Meteorological satellite experiments have mapped the earth in several wavelength regions of the electromagnetic spectrum. Two dimensional maps were generated which proved very useful for research as well as operational purposes. However, the most promising tool of modern meteorology, numerical forecasting by high-speed computers, must treat the atmosphere in three dimensions. Atmospheric processes in the troposphere are governed primarily by hydrodynamic forces. Integration of the Navier-Stokes equation or simplified forms of it require wind velocities, temperature profiles, water vapor distributions, cloudiness and surface pressure. Radiative heating and cooling are less important for short term forecasting, but influence the atmospheric processes over longer periods strongly. Today, only the surface temperature and cloudiness are under satellite surveillance.

The purpose of the IRIS experiment is to provide the temperature profile and the water vapor distribution. Wind velocities and surface pressure are still beyond the capabilities of remote measurements, but the potential to measure the surface pressure exists in measurements of the thermal emission spectrum. Besides the aforementioned goals, various other tasks can be accomplished by the IRIS experiment: ozone distributions, surface temperatures, and cloud height estimates may be derived from the data.

The above information will be extracted from the thermal emission spectrum within the interval of 2000 cm^{-1} (5 microns) to 500 cm^{-1} (20 microns) and possibly to 300 cm^{-1} (33 microns) with a spectral resolution of 5 cm^{-1}. The IRIS experiment is deliberately aimed at a wide spectral range to permit coverage of absorption regions of water vapor, carbon dioxide and ozone as well as the atmospheric windows.

Design considerations for the IRIS experiment are analyzed in detail. Spectral resolution, spectral range, and spatial resolution were influenced strongly by requirements to make the results available to numerical forecasting.

For Nimbus, the 8-degree field of view of the instrument covers a circle of about 160 km on the earth's surface, with the optical axis pointed toward the subsatellite point. Each spectrum is taken within 11 seconds. Image motion compensation is provided to eliminate smear. Calibration in orbit assures accuracy of measurement.

A Michelson-type interferometer is used in this experiment. A breadboard model of the instrument exists and is presently undergoing calibration and environmental tests. This report includes the design criteria for this interferometer and a detailed analysis of the achievable signal-to-noise properties.

The data reduction of the IRIS experiments requires a power spectrum analysis. Computer programs for this task were constructed and samples of simulated interferograms and analyzed spectra are shown.

Besides the application of the IRIS experiment to meteorology on earth, the same experiment and essentially the same instrumentation are capable of providing unique information on the atmospheres of Venus, Mars, Jupiter.

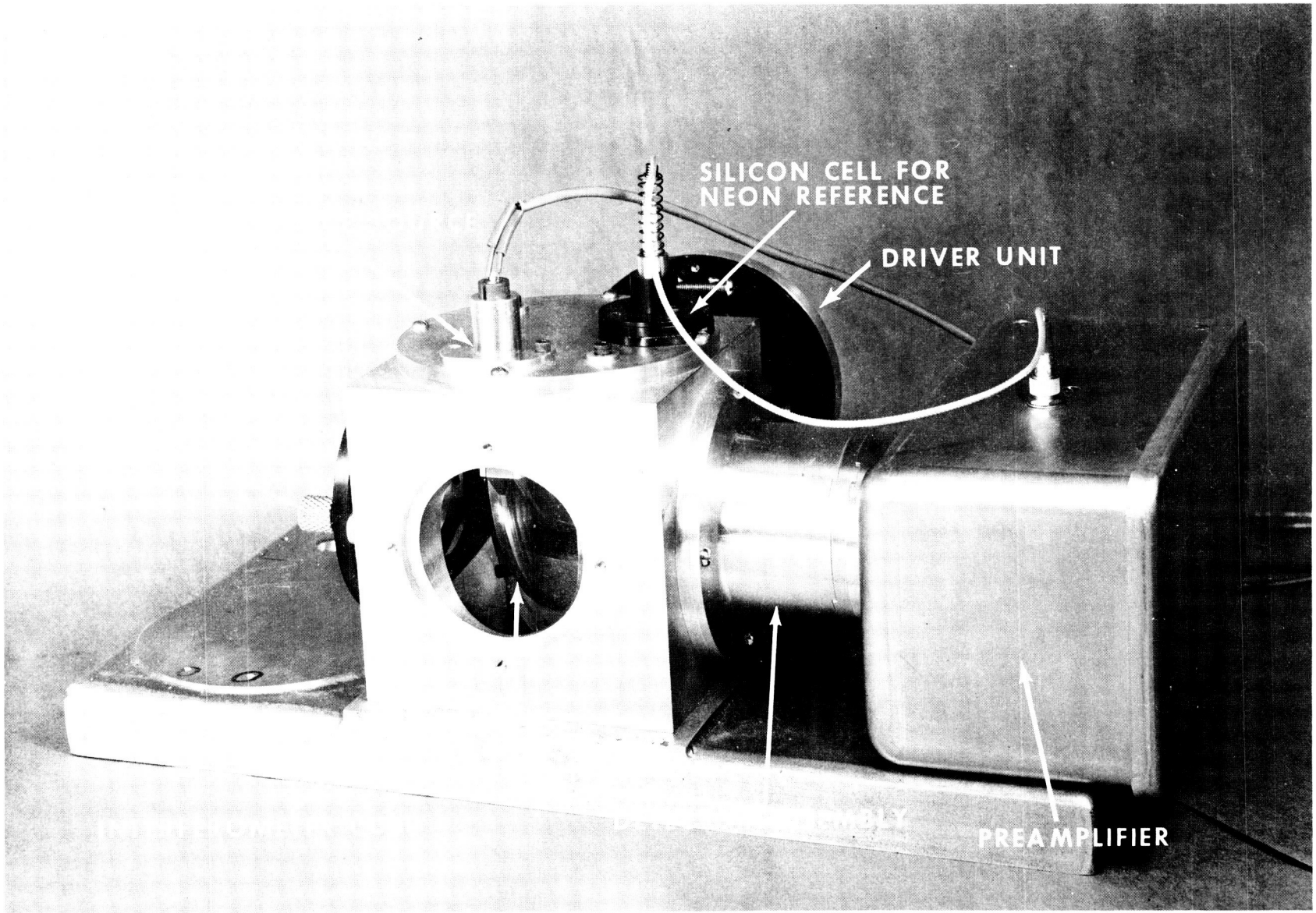

Frontispiece – Breadboard Model of Interferometer Cube

THE INFRARED INTERFEROMETER SPECTROMETER EXPERIMENT (IRIS)

(VOLUME II – METEOROLOGICAL MISSION)

INTRODUCTION

Scientific experiments have been performed from meteorological satellites since 1959. Vanguard II, Explorer VII, the TIROS series, and finally Nimbus are milestones on this road of increasing success. Mapping of the earth by television cameras and by infrared radiometers allows recognition of cloud patterns, identification of frontal systems, and tracking of major storms. The measurement of reflected solar radiation and thermal radiation emitted by the planet as a function of latitude and season provides data for the study of the heat balance and of climatology. Comparison of equivalent blackbody temperatures of the clouds as measured in the atmospheric windows (8-12μ or 3.5-4.1 μ) with climatological temperature profiles makes it possible to estimate the height of the upper limits of clouds. These early estimates and the more recent measurements of TIROS 7 in the 15μ CO_2 band were the first attempts to derive atmospheric parameters (cloudiness and temperatures, in this case) as a function of height. In general, however, radiometric mapping with relatively high spatial, but low spectral, resolution yields primarily cloud or moisture patterns in a two-dimensional sense but provides very little information on the vertical distribution of temperature, water vapor, or other parameters. Atmospheric motions, the vertical transport of moist air, and other meteorologically interesting phenomena can be recognized, described, and finally predicted only on a three-dimensional model. Mapping of the earth in wide spectral bands will continue to be a most useful meteorological tool; but, to understand the complex behavior of the atmosphere, a third dimension is required.

SCIENTIFIC OBJECTIVES OF THE IRIS EXPERIMENT

Basic Laws of Planetary Atmospheres

Planetary atmospheres tend to approach a state of thermal and mechanical equilibrium, so that atmospheric phenomena may be described by these equilibrium conditions and small deviations, if required. Terrestrial experience shows that even in strong storms the surface pressure fluctuates a few percent while temperatures between summer and winter vary less than ±10 percent. In general,

the atmosphere can be described on a gross scale by average or mean conditions combined with certain perturbations.

The initial reaction of a hypothetical gaseous envelope surrounding a planet would be its adjustment to mechanical or hydrostatic equilibrium; in other words, pressure forces will balance gravitational forces.

If the gas may be assumed to obey the perfect gas law, the pressure and density are then determined everywhere in the atmosphere. The temperatures are governed by the condition of thermodynamic equilibrium which requires the divergence of the energy flux to balance the energy sources. This net energy flux may be accommodated by various means of energy transport. Radiation, convection, heat conduction, diffusion, and even acoustical propagation of wind noise may participate in carrying the flux. Because many atoms and molecules in planetary atmospheres interact strongly with the radiation field, the radiative flux is very important. The radiative flux, which is always present, determines the thermal structure of large sections of the earth's atmosphere. When it is the only important mode of energy transport, a state of radiative equilibrium is achieved.

Sometimes, super-adiabatic temperature gradients are required to satisfy the flux divergence condition. The Schwarzschild stability criterion is then violated, and as a consequence, convective motions occur. The slow upward and downward transport of gas carries the convective component of the flux. The zone where convection supports the radiative transport, and determines the temperature distribution, is the zone of convective equilibrium. In general, the earth's stratosphere may be considered in radiative equilibrium and the troposphere in convective equilibrium.

However, on a rotating planet the equilibrium conditions may never truly be reached. The difference in the net flux between polar and equatorial regions requires lateral transport of energy which leads to horizontal motions, subject to Coriolis forces. On earth, solar radiation is partly used to evaporate water vapor while precipitation and evaporation create temporary sources and sinks of energy in the atmosphere. The complexity is further increased by the formation of clouds which influences the condition of thermal equilibrium strongly.

To deal with deviations from equilibrium, the simple treatment using the ideal gas law, the hydrostatic and thermodynamic equilibrium conditions is insufficient. The gas law must be augmented to account for the phase changes of water and the formation of clouds. The Navier-Stokes equation for a compressible, viscous medium must replace the hydrostatic condition. The Navier-Stokes equation is a nonlinear differential equation of second order which can only be solved by numerical integration.

The integration of the Navier-Stokes equation will gain further importance in meteorology. At present, numerical weather-prediction techniques are based on the integration of greatly simplified forms of this equation. To be truly useful for weather prediction schemes, satellite data must be applicable to the methods of numerical forecasting. This is discussed further in the chapter on design considerations for this experiment.

In the troposphere of the earth, the equilibrium conditions are of little interest. They are well known and only deviations from the average indicate the weather. In planetary atmospheres, however, the average conditions are not well known at all; therefore, equilibrium calculations and measurements serve very useful purposes.

The Thermal Emission Spectrum and Planetary Exploration

In the domain of the thermal emission spectrum of the earth and planets, a number of tasks can be performed. Some of these tasks such as the identification of gaseous constituents are very important for a study of the atmospheres of Venus, Mars, or Jupiter but are of little value to meteorology on earth. However, the known conditions on earth may serve as a proving ground for planetary experiments. Techniques as well as instrumentation may be tested.

Information about the distribution and total amount of some constituents (H_2O, e.g.) is equally important for the earth and the planets. The derivation of the temperature profile is again equally essential for the understanding of all atmospheres. The requirements on the accuracy, however, are more severe on earth, simply because more is known about our atmosphere than about the atmospheres of the other planets. The tolerances quoted in Table I give the order-of-magnitude of accuracy necessary to improve existing knowledge.

On earth the surface pressure must be measured very accurately if it is to be of any meteorological use, because only the small deviations from average are of interest. For Mars, on the other hand, one would be very happy to know the surface pressure within 10 percent. Clearly the earth and each of the planets have somewhat different requirements but it will be shown later that the instrumental requirements are more uniform than might be expected.

Temperature Profile

One objective of this experiment is to measure atmospheric as well as surface temperatures. Early investigators realized that the thermal emission spectra of stellar and planetary atmospheres contain information on the temperature profile. In 1956 King suggested the measurement of the limb function to determine

Table 1

Parameters Influencing the Thermal Emission Spectrum

	Earth	Venus	Mars	Jupiter
Identification of gaseous constituents	Not important, but proving ground for planetary experiments	Very important	Very important	Very important
Abundance and distribution of gases	Important for variables such as H_2O, O_3	Very important	Very important	Very important
Temperature profile	Very important required accuracy on the order of ±2°K	Important; lower accuracy acceptable, better than ±10°K	Important ±10°K	Important ±20°K
Surface or cloud-top pressure	Surface very important, extremely high accuracy required ±0.5% (±5 mb)	Cloudtop important ±20%	Surface very important for landing mission ±10%	Cloudtop important ±50%
Surface (cloudtop) temperature	Surface ±2° cloudtop ±2°	Cloudtop ±2°	Surface ±2°	±5°
Surface composition	Not important, but good proving ground	Not applicable	Very important	Not applicable

atmospheric temperatures on earth from a satellite and in 1959 Kaplan suggested a spectral scan in the 15μ CO_2 band for the same purpose. King's method suffers from the lack of horizontal stratification in the earth atmosphere. Kaplan's method has been given more attention – Wark (1961), Yamamoto (1961), King (1963), and others – and a spectrometer was designed specifically for this purpose (Dreyfus and Hillary, 1962).

Qualitatively the determination of the temperature profile is readily understood. The specific intensity emitted by the atmosphere originates from an atmospheric layer where the optical depth is about unity. Intensity is related to the true temperature by the Planck function (under the condition of local thermodynamic equilibrium); the atmospheric temperature can therefore be inferred from the intensity measurements. The resulting temperature is a weighted mean value for a relatively thick layer ($\sim$10 km). Using the intensity emitted in a spectral range of different absorption characteristics, the mean temperature of another layer may be obtained. In principle, then, the temperature distribution over a substantial portion of the atmosphere may be derived from measurements using a judicious selection of spectral intervals.

Quantitatively the above argument may be understood from the solution of the equation of radiative transfer.

$$I_{\nu\mu} = B_\nu(T_s)e^{-\tau_s} + \int_0^{\tau_s} B_\nu(\tau)e^{-\tau_{\nu\mu}} d\tau_{\nu\mu} \tag{1}$$

For a constituent of known and uniform mixing ratio, the optical depth is a known function of pressure in each spectral interval. In general, τ is a function of wavenumber, zenith angle, and the pressure and temperature corrected optical path. In the region of the atmospheric window, where the total optical depth to the surface is very small, the intensity is primarily given by the surface temperature, assuming an emissivity near unity. For opaque intervals, τ is large and the first term in the above equation contributes nothing. If the black surface is considered an isothermal extension of the atmosphere, equation (1) becomes

$$I_{\nu\mu} = \int_0^{\infty} B(\tau)e^{-\tau_{\nu\mu}} d\tau_{\nu\mu} \tag{2}$$

Over narrow wavenumber intervals $\Delta\nu$, B may be considered independent of ν.

Equation (2) is a Fredholm integral equation of the first kind and $e^{-\tau}$ is its kernel. The problem of finding the temperature profile requires the inversion

of equation (2). From the known kernel and the measured intensity, $B(\tau)$ is to be found. It is evident from the form of equation (2) that a scan in frequency (Kaplan) and a scan in viewing angle (King) are formally identical problems.

Small uncertainties in the measured intensities may result in oscillatory solutions of large amplitude; therefore, other criteria must be evoked to obtain a physically meaningful result. The problem is to apply sufficient smoothing to avoid instability, but not an excessive amount that would destroy the details inherent in the measurements. Several methods have been discussed in the literature on how numerical inversion can be applied to this problem – Kaplan (1961), Yamamoto (1961), Wark (1961), and King (1964). Flemming, Twomey and Wark (1964) and Drayson (1963) have performed error analyses and have shown that stringent requirements are placed on the absolute and relative accuracy of the intensity measurement.

To obtain four or eight temperature levels in the atmosphere, it is sufficient in principle to measure the specific intensity in four or eight narrow intervals, strategically located so that the individual absorption coefficients provide an optical depth of about unity at desired pressure levels. The interferometer yields a continuous spectrum and, therefore, contains inherently a higher degree of altitude resolution than measurements in individual spectral intervals. Some of this information will be redundant because the absorption coefficients in many spectral intervals will be approximately the same. A certain degree of redundancy, on the other hand, may be used to improve the accuracy.

The theory of the temperature sounding from satellites has been derived for absorbing atmospheres only. Scattering processes are usually avoided in calculations for reasons of simplicity. Atmospheric particles such as aerosols or cirrus clouds introduce difficulties which will have to be studied more thoroughly.

Water Vapor and Ozone Distribution

Suppose the analysis of the specific intensities in the 15μ band of CO_2 and in the atmospheric window has been performed, and the atmospheric temperatures are known down to the surface. Equation (2) may be integrated by parts and by a change in variables will produce:

$$I_\nu = B(\tau_\nu = 0) + \int_{T_s}^{T(\tau_\nu = 0)} e^{-\tau_\nu(T)} \frac{\partial B(T, \nu)}{\partial T} dT \qquad (3)$$

Aside from $B_{(\tau = 0)}$, equation (3) is formally identical to equation (2). The known kernel is now $\partial B/\partial T$ and one may solve for $\tau(T)$.

Numerical methods similar to those in the temperature problem can now be applied to a spectral region where water vapor or ozone are the major atmospheric absorbers, and their vertical distribution may then be obtained. Although error analyses have been performed on the temperature problem (Wark 1961, Drayson 1963), an error analysis on the determination of water-vapor distribution has not yet been carried out. However, preliminary calculations confirm the feasibility of this task. King (1963) has shown a method which derives mixing ratios without the explicit determination of the temperature profile.

Because of limited accuracy of stratospheric temperature estimates and greater uncertainties in the absorption characteristics, the ozone abundance and distribution are more difficult to determine. Earthbound and balloon-borne measurements of the ozone band and simultaneous stratospheric temperature soundings must supplement satellite-borne ozone soundings in the beginning.

The distribution of water vapor may be derived by studying the 6.3μ band or the rotational bands which show sufficient strength beyond 20μ. The ozone distribution may best be inferred from measurements near $9.6\,\mu$. The $14\,\mu$ ozone band is strongly blended by the 15μ CO_2 band and in addition is much weaker than the 9.6μ band.

Absorption coefficients for water vapor and ozone are available (e.g., Goody 1964). A verification of satellite data with simultaneous balloon soundings will occasionally be required to establish confidence in the conclusions.

As in the case of temperature soundings, clouds and aerosols introduce difficulties in the interpretations. The seriousness of these effects must be studied by experimentation from high-altitude balloons.

Surface and Cloudtop Temperatures

After the atmospheric constituents are identified, the effect of atmospheric absorption can be removed from the spectrum in those spectral ranges where the atmosphere is not opaque. The specific intensity emitted by the surface is then obtained:

$$I_\nu(\text{surface}) = \epsilon_\nu B_\nu(T_{\text{surface}}). \tag{4}$$

In the far infrared, most natural surfaces known on earth (rocks, gravel, plants, snow, etc.) have a high emissivity over large spectral ranges. However, the crystalline structure of complex molecules create stretching and bending resonances. For example, quartz exhibits strong stretching bands between 800 and 1100 cm^{-1} caused by the Si-O bond; other stretching groups (Si-Si) appear between 600 and 800 cm^{-1}. The same mineral has a bending mode (Si-O-Si) at 430 to 460 cm^{-1}. These resonances give a pronounced rise in the infrared reflectivity which can best be observed on polished samples. The increase in reflectivity is necessarily associated with a reduction in emissivity over the same spectral range.

The sharp rise in reflectivity has been well known since the early days of infrared studies. Rubens used the selective reflectivity of quartz plates to isolate narrow spectral bands in the far infrared. The reststrahlen phenomenon depends somewhat on the temperature of the sample and, to a much higher degree, on the surface roughness. Lyon (1963) has studied the emission and reflection spectra of many minerals in great detail. Deviations from an emissivity of unity in the region of the atmospheric window can cause errors in radiometric surface-temperature measurements. A high spectral resolution allows the identification of reststrahlen effects and therefore provides the means for improving the accuracy of surface-temperature measurements. This is also important for other radiometric, possibly scanning type, experiments especially over desert areas where SiO_2 reststrahlen phenomena may cause substantial errors.

If clouds are present, the cloudtop temperature is obtained instead. By comparison with the temperature measurement, the cloud altitude may be derived.

Other Investigations

Temperature sounding, the determination of the water vapor and ozone distribution, and the accurate measurement of the temperature of surface materials do not exhaust the potentials of the IRIS experiment. A few other possibilities shall be mentioned.

An accurate knowledge of the surface radiance and the atmospheric temperature allows, in theory, a derivation of the surface pressure. As King (1963) has shown, a region of weak CO_2 absorption may be used for this purpose. A preliminary investigation has shown that the required accuracies cannot be met at the present time; however, the task is important enough to be pursued further.

Minor atmospheric constituents such as N_2O (7.8; 9.56 and 17 μ) and CH_4 (7.66 μ) may be identified in the thermal emission spectrum. The weak absorption

of N_2O near 17 μ may be used to determine cloud altitudes in conjunction with the relatively transparent regions near 18 μ.

DESIGN CONSIDERATIONS FOR THE IRIS EXPERIMENT

Required Spectral Resolution

The identification of gaseous constituents requires high spectral resolution. It would be desirable to identify individual lines in the generally very complex spectra. In the P and R branches of the 15 μ CO_2 band, for example, individual lines have a separation of about 1.6 cm^{-1} and a line width of $\sim 10^{-1}$ cm^{-1}, depending on the pressure. To identify individual lines, an instrument would have to resolve to better than 0.1 of a wavenumber. For the earth's atmosphere, the identification of gases is not too important; however, the determination of the temperature profile requires the same order of resolving power. Unfortunately, small spacecraft instruments cannot now achieve this degree of resolution in the infrared.

The next best approach is to resolve the band contour as well as possible. Then a spectral resolution which is small compared to the total bandwidth is sufficient to identify a particular constituent. Similarly, for the measurement of the temperature profile, groups of lines may be selected. Kaplan (1959), Wark (1961) and others have shown that a five-wavenumber interval is sufficient. Smaller intervals do not yield further improvement unless one reaches 0.1 of a wavenumber or less and resolves individual lines. A five-wavenumber interval is within the feasible range for satellite instrumentation.

In summary, the goal of five-wavenumber resolution adopted for this experiment is a compromise between the desirable capability of 0.1 wavenumber and instrumental limitations. However, five-wavenumber resolution is a substantial improvement over space-borne techniques presently available and is sufficient to answer many pressing questions.

Required Spectral Range

The desired spectral range will be derived for the atmospheres of the earth as well as for other planets. However, only the region of the thermal emission spectrum where the reflected solar radiation is negligible will be considered.

- Earth

As pointed out earlier, a very interesting task will be the measurement of the temperature profile. Consequently the absorption spectrum of a uniformly mixed gas such as CO_2 should be included (15 μ). After deducing the temperature profile, the abundance and distribution of gases of variable mixing such as H_2O and O_3 may be obtained. Therefore, water-vapor and ozone absorption regions are of great interest (6.3 μ, 9.6 μ, and the rotational bands of water vapor). The surface or cloudtop temperatures may be measured in the atmospheric window between 10.5 and 11.5 μ, and this region should therefore be included in the desired range. Furthermore, if the surface and atmospheric temperatures and the surface emissivity are known, a region of intermediate CO_2 absorption may ultimately allow a direct determination of the surface pressure. However, present measurements are far from the required precision.

Except for small gaps, the whole thermal-emission spectrum yields significant information. Since the proposed interferometric method allows the coverage of a wide spectral region, and since the exclusion of certain gaps is more difficult than transmitting the whole spectrum, a record of the emission spectrum from 2000 cm^{-1} (5μ) to 500 cm^{-1} (20μ) is proposed. It would be desirable to cover the strong CO_2 bands near 4.2 μ, also, but the signal-to-noise ratio of the present instrument becomes very poor in this region. A response beyond 20 μ would also be desirable; the rotational water-vapor band would be superior over the 6.3μ region from a signal-to-noise point of view, but other instrumental considerations (materials for beam splitter) impose limits there. The spectral region of the instrument will hopefully be extended to 30μ in the future.

- Venus

The abundance of CO_2 on Venus makes the measurement of the CO_2 bands very important including the weaker bands of CO_2 near 9.4 and 10.4 μ. Water-vapor absorption in the 6.3μ band would be sufficient to confirm present estimates on the water vapor content above the clouds. Today, nothing is known about the thermal emission of Venus between 12 and 100μ where 75 percent of the thermal energy lies. Besides the search for known or expected phenomena, a search for unexpected spectral features is most important. Therefore, a wide spectral range should be the design goal for a Venus fly-by experiment.

- Mars

Similar arguments hold for a possible exploration of Mars. In addition to the identification of atmospheric constituents, "reststrahlen" phenomena in

surface materials may allow their identification. Again, a search for unexpected features requires a wide spectral range (Hanel and Chaney, 1964).

- Jupiter

The atmosphere of Jupiter contains large quantities of hydrogen and helium, but neither molecule shows resonances at moderate pressures in the far infrared region. However, other constituents such as NH_3 and CH_4 have strong molecular absorption bands in the 5 to 30 μ range. Again, a wide spectral range is most desirable.

In summary, a wide spectral range of the instrument is most desirable for application to the earth's atmosphere for meteorological purposes and for planetary exploration from fly-by vehicles. As mentioned before, the design goal encompasses a spectral range from 5 μ (2000 cm^{-1}) to 20 μ (500 cm^{-1}) with a possible extension to longer wavelength.

The wide spectral range does create challenging problems in the design of the instrument, primarily in two areas: One concerns the beam splitter, which has to operate properly over the wide range. The other problem is in the large dynamic range of the signal which must be digested by the data transmission channel. As discussed later, both problems have been solved satisfactorily.

Required Spatial Resolution in the Horizontal and Vertical

Weather prediction by numerical integration of the Navier-Stokes equations, or simplified forms of it, requires the knowledge of certain initial conditions. Initial conditions reflect the state of the atmosphere at a particular time and consist ideally of the wind velocities, the temperature profile, the water vapor content, and the surface pressure. For short time forecasting, on the order of a few days, atmospheric heating processes are less important than the aforementioned parameters (Mintz 1963). With the exception of the surface temperature, and those rare occasions when the wind velocities can be inferred from cloud patterns or from the size of the sun's image reflected from water, neither of the necessary parameters is measured by meteorological satellites today. Wind fields and surface pressure are still beyond the realistic capabilities of remote measurements, but the temperature profile and the water vapor distribution are within the potential of this experiment.

For longer range forecasting, the time-dependent heating or cooling of the atmosphere also becomes important. Surface temperatures and cloudiness are main factors. Both these parameters, in addition to the total radiative heat loss,

are already under satellite observation or can be inferred from the results of such observation.

Present techniques for numerical forecasting are still relatively crude. The finite storage capability of today's computers limits the number of atmospheric volume elements which can be considered simultaneously. As discussed by Mintz (1963), the lowest useful resolution uses a two-layer model of the atmosphere with a horizontal dimension of 1000 km per element. This type of element is still small compared to the characteristic wavelength of cyclonic motions. Surprisingly, numerical integration of the so-called primitive equations yields very good results using a two- or four-layer atmospheric model with a horizontal element size of only 800 km (Mintz, 1964).

These considerations are useful for comparison with the minimum spatial resolution requirement for the interferometer experiment. Spectral resolution and wavelength range limit the maximum field-of-view of the interferometer to about 8 degrees. This is discussed in detail later. At the nominal altitude of Nimbus (1100 km), this field-of-view corresponds to a circular area of about 160 km diameter. The horizontal resolution of this instrument is therefore much better than the element sizes required for numerical forecasting. The interferometer will be used without additional optical elements on Nimbus. Other applications such as planetary fly-by missions from greater distances, or observations from synchronous altitudes on earth, require a telescope to take full advantage of the light gathering power of the interferometer and simultaneously restrict the overall field of view to less than 8 degrees.

The number of vertical layers for which the temperature and water vapor content should be derived must again be determined by the number of layers that the numerical models of atmospheric behavior can digest. From the present state-of-the-art of numerical forecasting, it is concluded that four or perhaps eight layers distributed equally over pressure, if possible, should be ample.

Dynamic Range

The IRIS instrument, like all radiometric devices using thermal detectors, responds to the difference between the radiance of the target and its own radiant emission. Three principal modes of operations are possible: The instrument temperature can be chosen either entirely above or below the target temperatures, or near the center of the dynamic range. Operation at either temperature extreme avoids ambiguities in the interpretation of the spectra at the expense of the required dynamic range. Since outer space will be used as a convenient almost zero-degree calibration target, operation below target temperatures is impossible.

Operation above the maximum of expected blackbody temperatures (320°K in window over desert) is undesirable, because of the wide dynamic range required and because of noise considerations in the detector. Therefore, an operating temperature at 250°K was selected. Under these conditions the emitted radiation during calibration approximately equals the received net radiation from the warmest target (300°K). It is sufficient to design for the maximum average blackbody temperature which may be encountered, rather than for the peak, since phase reversals are permitted. However, the insensitivity of the power spectrum to the relative "phase" of the individual frequency components in the interferogram leads to an ambiguity. The power spectrum was selected rather than a pure cosine transformation for this very reason. We do not wish to depend on the phase characteristic of the system and the lack of dispersion in the beam splitter. On the contrary, a moderate dispersion is desired since it reduces the high central peak in the interferogram.

In general, the ambiguity can be resolved by an a priori knowledge of the shape of the spectrum; however, in automatic modes of data processing, a more definitive criterion is required. This criterion exists in the difference in "phase" of two adjacent frequency components; if they appear "in phase" near the center region of the interferogram, the corresponding blackbody temperatures are both warmer or both cooler than the instrument temperature. An accurate knowledge of the position of the central peak is not required. Because certain parts of the spectrum such as parts of the 15μ CO_2 band will always be cooler than 250°K, the ambiguity is resolved. The relative "phase" of the individual frequency components is obtained from the sign of the sine and cosine amplitudes which are squared and summed to yield one data point in the power spectrum.

THE INTERFEROMETER SPECTROMETER

The instrument, basically a Twyman-Green modification of the Michelson interferometer (Figure 1), departs from the classical laboratory designs in several areas:

- The drive mirror is suspended by a parallel leaf-spring system.
- The mirror assembly is driven by a moving coil in a strong magnetic field; a second coil generates a voltage proportional to the mirror speed which is used to control the mirror speed by feedback.
- The mirror motion is monitored by an auxiliary interferometer to assure proper sampling times.
- The compensating plate is moved to a position adjacent to the beam splitter.

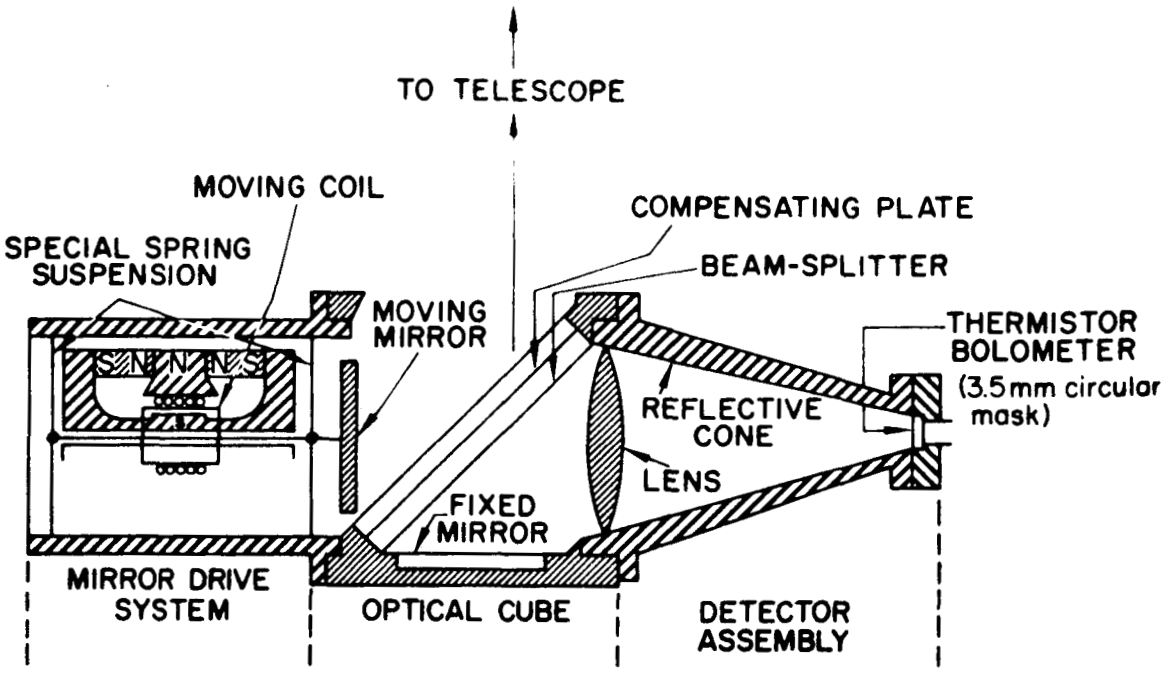

Neon Light Source and Auxiliary Detector for 5852 Å Reference Line Not Shown

Figure 1 – Interferometer Cube, Mirror Drive Assembly, and Detector Assembly: Schematic Diagram

This particular configuration of the interferometer was chosen because of its inherent compactness, large light-gathering power, and design simplicity.

Radiation arriving within the field-of-view is divided by the beamsplitter into two components which recombine and interfere after reflections on the fixed and moving mirrors respectively. The recombined beam, focused on the detector, is modulated by the motion of the scan mirror proportional to the speed of the mirror and the wavenumber of the incident radiation. The output signal from the detector, called the interferogram, is the Fourier transformation of the spectrum of the incident radiation. The signal is amplified, digitized, and transmitted over the spacecraft telemetering system. On the ground, the spectrum is reconstructed by applying the inverse transformation. The original spectrum can be precisely reconstructed only within certain limits of accuracy of spectral range and of spectral resolution.

Theory of Fourier Spectroscopy

Interference spectroscopy, first suggested by Michelson after the development of his original interferometer, was not pursued because of extreme computational difficulties, and further development was forced to wait upon the advent of electronics and high-speed digital computers. In the last decade, interference spectroscopy has made great advances; work has been reported by Fellgett (1958), Gebbie (1959), Mertz (1956), Connes (1961), Strong and Vanesse (1959), Loewenstein (1963), and many others. Excellent summaries may be found in articles by Jacquinot (1960) and by Connes (1961).

The source of radiation for the interferometer will be an extended target which completely fills the field-of-view with radiation passing through the instrument without collimation. The output fringe pattern of the interferometer is focused on the detector, which is masked to eliminate all but the central fringe. The output of the detector is amplified and recorded as a function of path difference, d, between the fixed and movable mirror.

The relationship between the effective path difference, the order of interference, and the radiation wavelength is

$$m\lambda = 2d \cos \theta$$

where

d is the path difference between the two interferometer paths (cm)

m is the order of interference

λ is the wavelength (cm)

θ is the angle of an oblique ray through the interferometer.

This expression shows that, for a given monochromatic signal of wavelength, λ, the circular fringe corresponding to a given order m expands away from the center of the pattern as the separation of the mirrors is increased. The detector is mounted behind the mask so that only the central fringe is detected; each spectral element is thereby modulated sinusoidally at a rate inversely proportional to its wavelength. As the source has an appreciable range of spectral elements, the signal detected will be the superposition of many modulated intensities multiplied by a parameter which is the "responsivity" of the system; i.e.,

$$\phi_{(x)} = \frac{1}{2}\int_0^\infty K_\nu N_\nu \, d\nu + \frac{1}{2}\int_0^\infty K_\nu N_\nu \cos 2\pi\nu x \, d\nu$$

where N_ν is the spectral radiance of the source (assumed to be the same at all parts of the field-of-view)

ν is the wavenumber, cm^{-1} ($\nu = 1/\lambda$)

x is the instantaneous value of the effective path difference of the two beams of the interferometer (cm)

K_ν is a parameter which expresses the effective spectral responsivity of the interferometer, including the characteristics of the optics, the detector, and the electronic amplifiers

The interferogram is then taken to be

$$I_{(x)} = 2\left[\Phi_{(x)} - \frac{1}{2}\Phi(0)\right]$$

$$= \int_0^\infty K_\nu N_\nu \cos 2\pi\nu x \, d\nu,$$

which is the Fourier cosine transform of $K_\nu \cdot N_\nu$. The product $K_\nu \cdot N_\nu$ can be obtained uniquely from the measured interferogram, taking the inverse transform by digital computation. The relationship between N_ν and the product $K_\nu \cdot N_\nu$ will be established by laboratory calibrations; the validity of the laboratory calibrations is established by in-flight calibrations.

The true spectral distribution $K_\nu \cdot N_\nu$ is found only when the interferogram is recorded for an infinite range of x. For a finite range of x, each spectral component is spread out into a shape known as the instrumental profile. This profile also depends on the obliquity of rays through the interferometer, and thus on the solid angle of the field-of-view. The instrument profile may be modified as desired during computation of the transform; this process, called apodization, usually is done to remove secondary maxima at the expense of resolution.

Including all these effects, the expression for the interferogram becomes

$$I_{(x)} = \int_0^\infty N_\nu \cdot s(\nu, x) \cdot \cos\left[2\pi\nu x + \phi(\nu, x)\right] d\nu,$$

where

$$S(\nu,x) = s(\nu,x)\ \exp[i\phi(\nu,x)]$$

is the Fourier transform of the instrument profile (including the parameter K_ν mentioned previously).

The spectral distribution is again obtained by computing the Fourier transform of $I_{(x)}$. Reconstruction of the spectral distribution of the source N_ν is obviously an approximation of the actual spectral distribution. This approximate solution (i.e., the transform of the interferogram) is the convolution of the actual spectral distribution with the instrument profile; therefore, it is mandatory to determine the form of the instrument profile. This can be done experimentally, because the instrument profile is the apparent spectral response of the instrument to a monochromatic source. This determination of the instrument profile is an important part of the laboratory calibrations.

Two factors which influence the instrument profile and reduce the quality of the data are the limitation arising from the finite path of the movable mirror, and the effect of oblique rays through the interferometer. The resolution limit imposed by the finite-path limitation is

$$R = \nu L \text{ or } \Delta\nu = \frac{1}{L} \ ,$$

(assuming linear apodization to remove secondary maxima in the instrument function). The resolution limit imposed by oblique-ray effects is

$$R\Omega = 2\pi, \quad \text{or} \quad \Delta\nu = \frac{\nu\Omega}{2\pi} \ .$$

In the above, R is the resolution $\nu/\Delta\nu$, L is the maximum path difference on either side of zero path difference, and Ω is the solid-angle field-of-view of the interferometer.

- Advantages of the Interferometer

An analysis by Jacquinot indicates that, where a source whose spectrum is defined by a radiance N_ν, having M spectral elements of interest, is to be analyzed with a resolution R in a time T with an optical system which is detector-noise-limited (as presently in the infrared), then the signal-to-noise ratio is increased by maximizing the time t of observation of each spectral

element, the admissible solid angle Ω, and the transmission factor ϵ_ν (the optical efficiency).

An interferometer fulfills these requirements to a high degree. The time of observation is $t = T(m/M)$,, where m is the number of spectral elements studied simultaneously. For an interferometer, m equals M, and m/M has the maximum value 1. The luminous energy received by the detector is $N_\nu \cdot A \cdot \Omega$. The quantities A and Ω can both be made large for an interferometer, as long as the resolution limitation $R\Omega = 2\pi$ is not exceeded (for comparison, the same resolution limit for a grating spectrometer is $R\Omega < 0.1$). The transmission factor • is the only area where the superiority of the interferometer may be questioned for a given application. The reflectivity and transmissivity of the beam splitter is of primary importance, and it may be difficult to obtain high efficiency from mechanically suitable materials in certain portions of the infrared spectrum.

Mechanical and Electromechanical Design of Breadboard Instrument

The instrument for the IRIS experiment consists of:

- interferometer (cube, detector, mirror-drive system, preamplifiers)
- 45-degree mirror rotating to reflect outer space and a blackbody during in-flight calibration and to provide image-motion compensation
- electronics compartment, containing all electronic circuits except for the preamplifiers in the cube and electronics located in calibration mirror assembly
- mechanical structure to receive the interferometer, the calibration target, the calibration mirror, and to provide mechanical strength and thermal protection

The electronics compartment, located separately, is connected to the interferometer assembly by a cable.

The mechanical design of the interferometer is modular. The drive unit, the fixed mirror assembly, the detector assembly, and the monochromatic reference source-detector combination are integral components attached to the optical cube, which houses the beam splitter and provides mechanical strength and thermal conduction to all components.

The scan mirror is one of the most critical items in the design because it must be moved through a distance of 2 mm with a total angular rotation of less than 2 seconds of arc.

The use of parallel leaf springs to support the mirror was chosen in preference to slides on ways, or pivot-point mounts, since it avoids frictional surfaces undesirable in space applications. The driving force is generated by an electrical current in a moving coil in a strong magnetic field. As Figure 1 shows, the magnetic gap is inside the dual-magnet design, thus minimizing residual magnetic fields on the outside.

Lack of uniformity in drive-mirror speed normally produces catastrophic effects on the wavenumber calibration of interferometers. Two methods used to eliminate virtually all errors and uncertainties in the mirror motion, and in the subsequent wavelength calibration, are based on the use of an auxiliary interferometer and a feedback control of the mirror drive:

- A monochromatic source (0.5852 micron) feeds the interferometer and generates a sinewave at an auxiliary detector. The frequency of the sinewave is directly proportional to the speed of the mirror. Sampling times of the interferogram are derived from this reference frequency.

- The mirror velocity is maintained constant to ±1 percent by energizing an electromechanical drive coil from an error amplifier that compares a reference voltage to a voltage proportional to the mirror velocity. The latter voltage is derived from a pickup coil attached to the mirror mount that moves through a constant magnetic field. This method also provides electromechanical damping in the neutral position of the mirror (with zero reference voltage) which is very important during the launch phase.

Optical Design of the Breadboard Instrument

The optical design of the interferometer is conventional. The flat mirrors and the detector determine the limiting apertures. The condition of optimum solid angle $R\Omega = 2\pi$ is fulfilled at the highest wavenumber to be analyzed ($2000\ cm^{-1}, 5\ \mu$). The optimum angle is then 8 degrees (±4 degrees) for a resolving power of 400 ($5\ cm^{-1}$ at $2000\ cm^{-1}$).

The fixed mirror and the scan mirror are made of gold-coated quartz polished to a flatness better than $0.1\ \mu$. Gold was selected because of its stability

and its high reflectivity in the infrared. The two-axis mirror mount is machined from a single piece of metal. A differential screw which produces the fine adjustment required also anchors each adjustable plane at three points.

The condensing optic consists of a KBr lens, combined with a gold-coated reflective cone which increases the effective detector area. Dimensions are chosen to provide the 8-degree acceptable angle. The f-number of this system will approach the ideal limit of 0.5.

The bolometer in this design is essentially an integral part of the condensing optic. The detector is a 3.5-mm square masked to a circle of 3.5-mm diameter, having a time constant of 1 millisecond.

The beam splitter is the most critical item in the optical train. All the rays make two passes through the beam splitter; hence, all the losses arising in this unit are doubled. Although metallic beam splitters are preferable from the standpoint of uniformity with wavelength, they have the serious disadvantage that absorption losses are high. Dielectric beam splitters cannot be made uniform with wavelength, but over the wavelength span of interest the efficiency will be at least equal to that of a metallic splitter. The dielectric material selected is germanium, which has the additional advantage of being highly reflective for wavelengths shorter than 2μ, so that most of the reflected visible radiation will not be collected.

The substrate material used in the breadboard instrument is KBr. Other materials currently being investigated for their suitability as beam splitters include IRTRAN-4, KRS-5, CsI, and plastic pellicles.

The radiation source for the monochromatic reference signal is the 0.5852 μ neon line, which is quite strong; in conjunction with a suitable interference filter, the signal is suitably monochromatic. Neon was selected because lamps are available in small sizes and very little power is required. The focusing and condensing optics are all glass of conventional and straightforward design. A silicon photovoltaic cell serves as a detector.

Electronic Design of the Breadboard Instrument

The electronics for the IRIS instrument are designed to perform the functions necessary to control the interferometer and process the data presentation to the spacecraft. The design consists primarily of digital electronics, because of the inherent reliability of these systems. The digital circuits are constructed of Texas Instrument modules. This subsystem is a self-contained instrument

requiring a minimum of external control for the operation of the experiment. A reliability survey will be conducted as one of the system evaluation parameters.

The electronic circuitry for the interferometer is designed to operate as independently of the spacecraft as possible. The spacecraft supplies the power and command signals necessary to operate the experiment; the electronics subsystem of the experiment processes the interferometer data and presents them to the spacecraft in a digital format. The spacecraft supplies a single command at the beginning of each interferometer frame, but the necessary sequence of events to complete the data frame is generated by the interferometer system.

Functions of the interferometer electronics (Figure 2) are:

- To amplify the thermistor-bolometer output signal
- To sample the bolometer signal and present it to the spacecraft telemetry system in serial digital form
- To provide the necessary control to drive the moving mirror at constant speed (±1 percent)
- To provide a calibration sequence and controls for image-motion compensation
- Convert the -24.5v spacecraft power into voltages required to operate the interferometer

The data channel receives as an input the 0 to 1.0-volt peak analog signal from the thermistor bolometer preamplifier. This electrical signal is band-limited between 10 cps and 100 cps in an electrical filter network, 12 db/decade.

The signal amplifier has a voltage gain of 36 db. The band-limited electrical signal is coupled through the switched attenuator (0, - 20 db) into the signal amplifier. The state of the switched attenuator is controlled by a comparator circuit that senses the level at the output of the signal amplifier, as shown in Figure 2. The attenuator has two positions, controlled by the level of the preamplifier output voltage: 0-db attenuation and 20-db attenuation. The preamplifier output fed into a comparator generates an output to switch in the 20-db attenuator when the preamplifier output exceeds ±3.2 volts, and to switch out the attenuator when the signal falls below ±0.32 volts. The gain change is necessary to accommodate the extremely large dynamic range (1500:1) of the input signal from the bolometer preamplifier. The output of the bolometer preamplifier is maintained between 0 and -6.4 volts, a value compatible with the analog-to-digital converter.

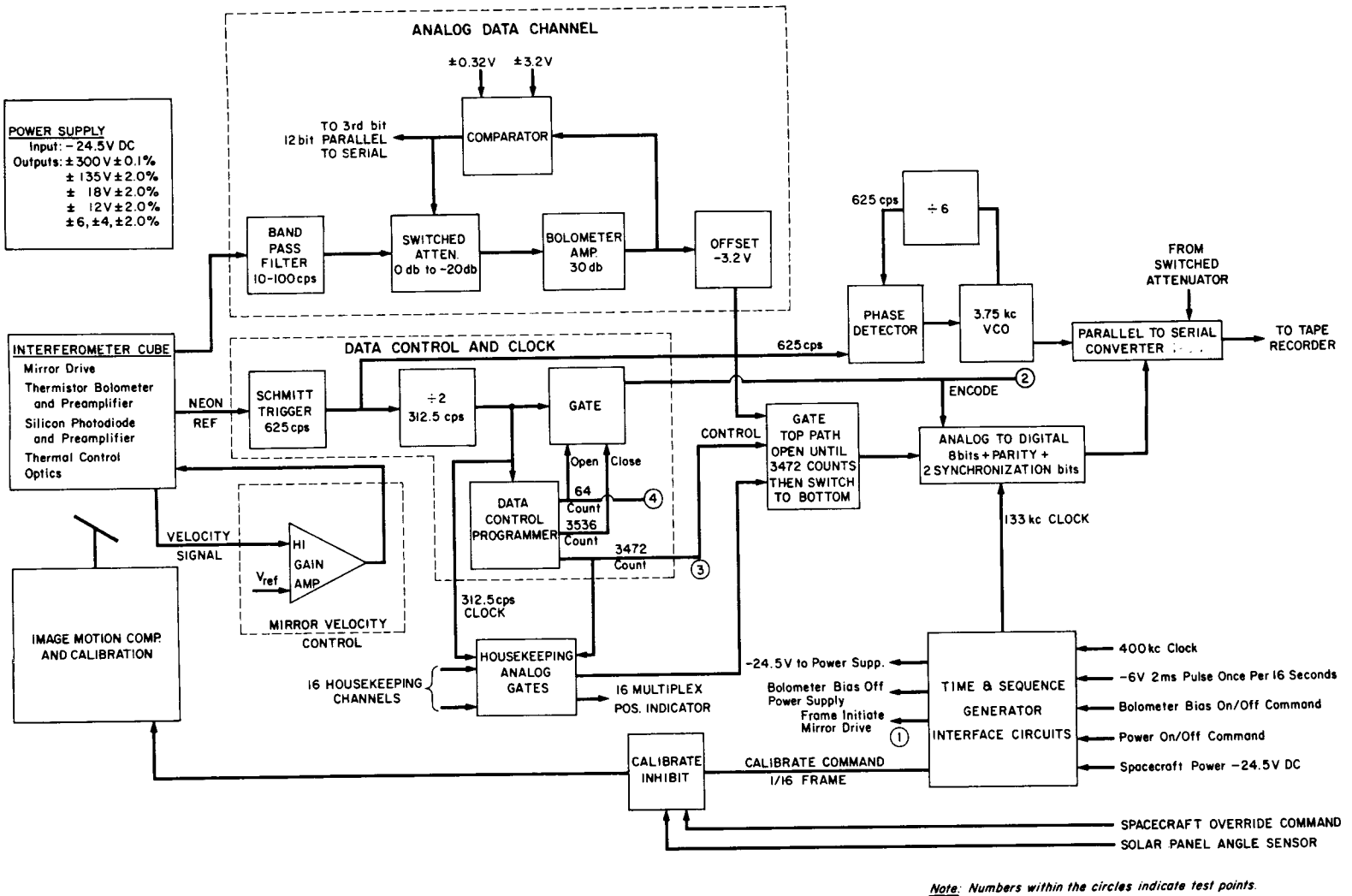

Note: Numbers within the circles indicate test points.

Figure 2 – Interferometer Electronics, Block Diagram

The function of the data control channel is to:

- Provide the necessary encode pulses to the analog-to-digital converter at proper mirror positions
- Ensure that data points are not transmitted until the mirror velocity has stabilized
- Allow precisely 3408 data points for each data frame
- Allow 64 additional pulses to cycle through the 16 housekeeping telemetry points four times

The encode pulses to the analog-to-digital converter are derived from the auxiliary interference of the neon reference. This ensures that the data samples are taken at specific mirror positions rather than at equal intervals of time. This precaution is taken to remove the effect of small mirror-velocity variations.

The count-to-128 logical output inhibits data flow from the experiment until the mirror velocity has stabilized. After this time, the 312-1/2 cps neon interference signals are coupled to the analog-to-digital converter as encode pulses.

The logical output from the count-to-3408 switches the operation of the instrument from the infrared data to the housekeeping data. The 16 housekeeping channels are cycled through four times, and the instrument is switched off.

The telemetry output unit receives the digital data from the analog converter and electronics in the form of a 12-bit word. The word consists of the 8 bits from the analog-to-digital converter and a parity bit, a single bit indicating the state of the 20-db attenuator, and two bits used for word synchronization. These data are transferred to the spacecraft tape recorder by a clock that is phase-locked to the neon interference signal.

The function of the mirror-control circuitry is to drive the Michelson mirror at a constant velocity for the duration of one experiment. The design goal for the mirror-velocity control servomechanism is for a velocity of 0.185 mm/sec ±1 percent for a displacement of about 2 mm. The velocity is kept constant by controlling the current in an electromechanical drive coil attached to the moving mirror. This current is derived from an operational amplifier coupled to a reference voltage and a voltage proportional to mirror velocity. This voltage proportional to velocity is generated in a pickup coil attached to the mirror mount that moves through a constant magnetic field.

The 45-degree scan mirror compensates for image motion to ensure that the same scene is viewed during the 11-sec interval of each interferogram. In addition to providing motion compensation, this scan mechanism provides calibration signals. During calibration the scan mirror is rotated to bring a thermally controlled (300°K) blackbody into the field-of-view of the instrument. After obtaining the calibration interferogram, the scan mirror rotates 90-degrees to bring outer space (0°K) into the field-of-view and a second calibration interferogram is recorded. This constitutes calibration for both extremes of the instrument. The calibration sequence, which will be initiated after every 14 interferograms (every 16th frame-initiate command), is inhibited by a signal from the solar panel position indicator to guard against damaging the sensor by projecting the solar image on the detector.

The power supply is a standard type of dc-to-dc converter. The raw voltage, necessary to operate the instrument are regulated to ±5 percent, sufficient for proper operation. In addition two reference voltages are regulated to ±0.1 percent. Outputs from the power supply are:

- ±300v ± 0.1 percent thermistor bolometer bias supply
- 12v ± 0.1 percent reference voltage – mirror drive
- ±18, ±12, ±6, ±4v at 2.0 percent regulation

Signal-to-Noise Ratio

The peak signal falling on the detector (for zero path difference) is

$$P = \frac{1}{2} N \cdot A \cdot \Omega \cdot \epsilon .$$

where

P = radiant power (watts)

N = target radiance (watt cm^{-2} $ster^{-1}$)

A = effective aperture (cm^2)

Ω = solid angle (ster)

ϵ = average optical efficiency

The factor 1/2 accounts for the 50-percent reflection losses inherent in this type of interferometer. The noise at the detector is given by the noise-equivalent power (NEP) of a thermistor bolometer, which is approximately

$$\text{NEP} = 1.6 \cdot 10^{-10} \sqrt{a} \sqrt{\frac{\Delta f}{\tau}},$$

where

a = area of detector (cm^2)

Δf = noise bandwidth (cps)

τ = detector time constant (sec)

Additional noise will be contributed by the compensating thermistor ($\sqrt{2}$), noise in the bias supply ($\sqrt{2}$), and preamplifier noise ($\sqrt{2}$). For operation at 250°K the NEP is lower; however, this improvement will not be considered here.

The peak signal-to-RMS noise ratio in the interferogram, for zero path displacement, is then

$$\frac{S}{N} = \frac{P}{\text{NEP}} \approx 10^9 \text{NA}\Omega\epsilon \sqrt{\frac{\tau}{a\Delta f}}.$$

The signal power in the spectral interval $\Delta\nu$ will be approximately equal to the peak power P times the ratio $N_\nu \Delta_\nu \epsilon_\nu / N\epsilon$. In addition, a signal-to-noise improvement factor proportional to $\sqrt{n/2}$ (n = number of samples per interferogram) is obtained; therefore,

$$\left(\frac{S}{N}\right)_{\Delta\nu} \approx 10^9 N_\nu \Delta_\nu \epsilon_\nu A \cdot \Omega \sqrt{\frac{\tau n}{2a\Delta f}}.$$

The square root of n/2 is used instead of $\sqrt{n}$, because about half of the samples are redundant.

Assuming reasonable numerical values for some parameters,

effective aperture A = 10 cm^2

solid angle Ω = $1.57 \cdot 10^{-2}$ (8°)

optical efficiency $\epsilon \approx \epsilon_\nu$ = 0.2

detector time const. τ = 1 ms

detector area a = .1225 cm^2

number of samples n = 3408

spectral element $\Delta\nu$ = 5 cm^{-1}

noise equivalent bandwidth $\Delta f \approx$ 136 cps

the peak signal-to-noise ratio becomes

$$\frac{S}{N} = 2.5 \cdot 10^5 N,$$

and for a spectral interval

$$\left(\frac{S}{N}\right)_{\Delta\nu} = 5 \cdot 10^7 N_\nu.$$

The instrument temperature (250°K) was chosen to give approximately equal signals for the maximum blackbody temperature to be measured (300°K), and for outer space (0°K), which is used as a check of calibration. The maximum radiance between 500 and 2000 cm^{-1} is about $6.2 \cdot 10^{-3}$ watt cm^{-2} $ster^{-1}$ (300°K); therefore, the maximum signal-to-noise ratio is about 1500.

Within the spectral intervals, the signal-to-noise ratios depend largely on spectral radiance. A plot of N_ν for various blackbody temperatures is shown in Figures 3 and 4; in both cases, the instrument is at 250°K. However, before the final signal-to-noise ratio can be discussed realistically, errors in the coding process must be taken into account.

The most efficient way to encode is to set one coding step equal to the rms value of the noise in the interferogram. Higher coding accuracy yields insignificant improvement; lower coding accuracy is undesirable. If encoding is performed to 1 part in 1500 of the maximum possible amplitude in the interferogram, the uncertainties introduced by the coding process will equal errors caused by detector noise. The final signal-to-noise value, including the coding error, becomes

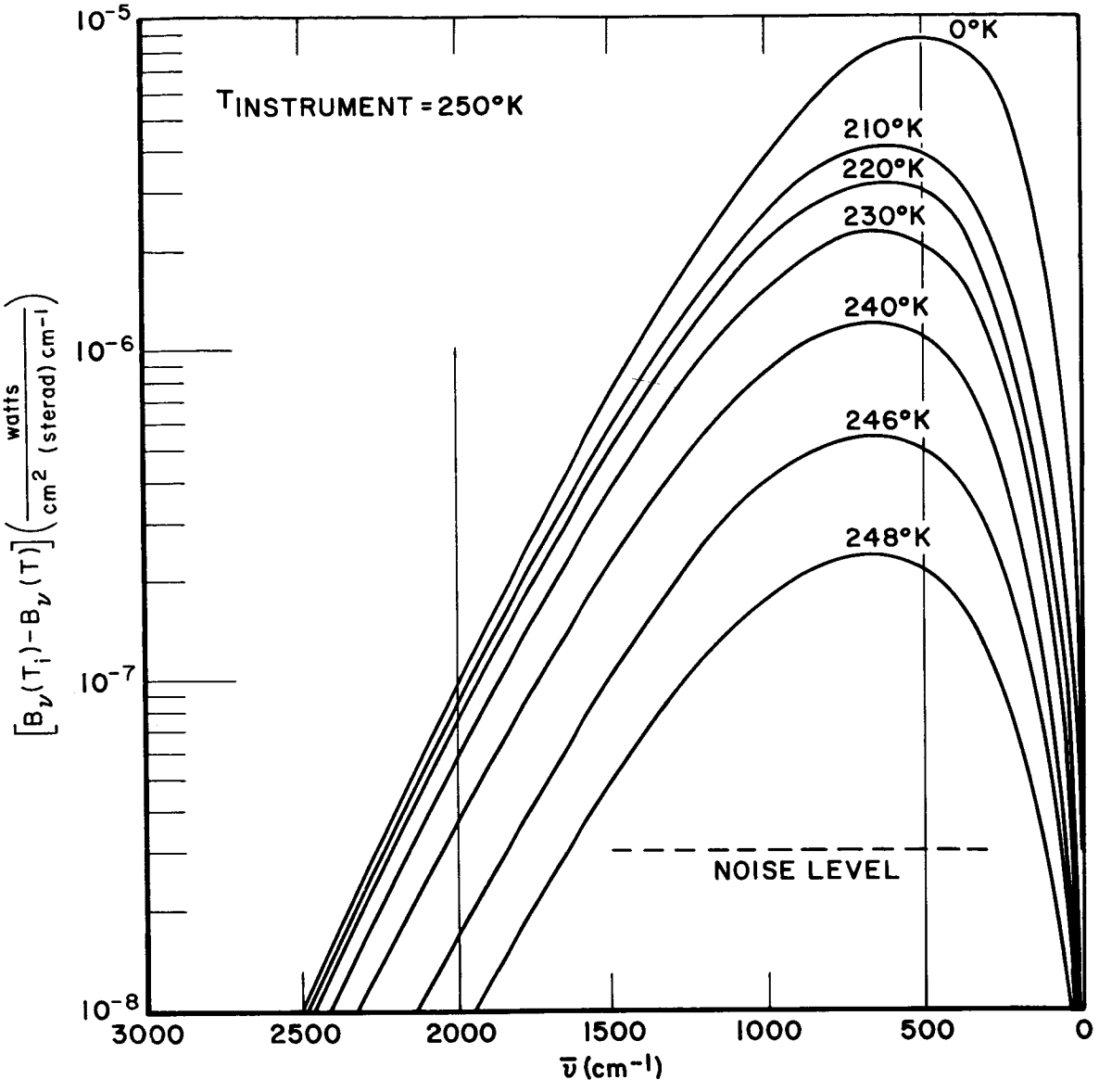

Figure 3–Difference in Spectral Radiance of a Target Colder Than the Interferometer

$$\frac{S}{N} = 1.7 \cdot 10^5 N \text{ and } \left(\frac{S}{N}\right)_{\Delta\nu} = 3.5 \cdot 10^7 N_\nu.$$

A $(S/N)_{\Delta\nu}$ equal to unity is obtained for $N_\nu = 3 \cdot 10^{-8}$. This value is indicated in Figures 3 and 4. A temperature difference of 2°K should therefore be detectable below 1650 cm^{-1} (above 6 microns); at 1850 cm^{-1} (5.4 microns), 4°K corresponds to the noise, and at 2000 (5 microns) only about 8°K.

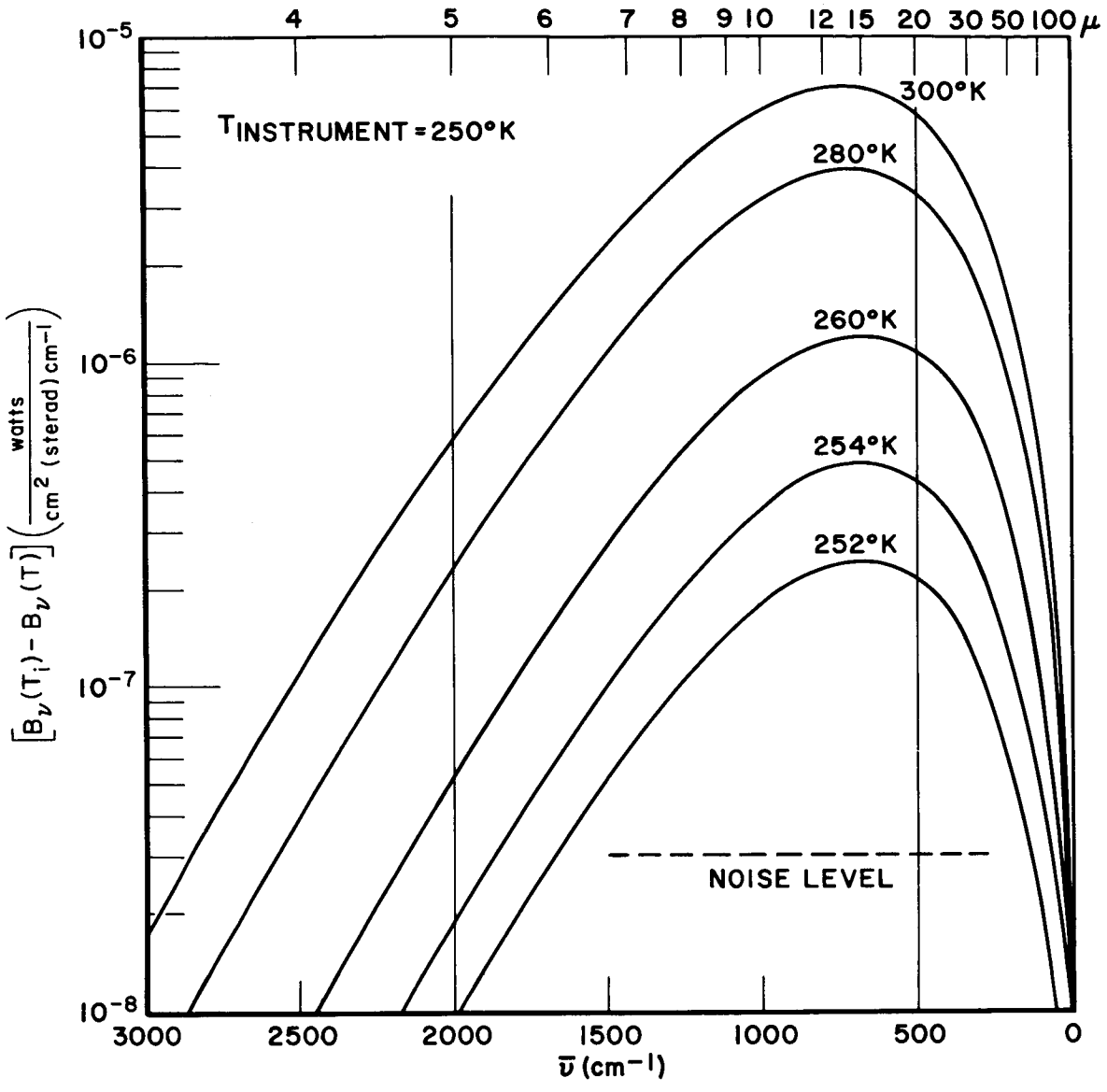

Figure 4–Difference in Spectral Radiance of a Target Warmer Than the Interferometer

These numbers were derived for 5 cm^{-1} resolution. Clearly, numerical smoothing techniques can be applied and resolving power can be traded against accuracy. This operation is done on the ground after the interferogram has been received, so that considerations of this nature do not influence the design of the instrument.

It remains to be shown how a signal-to-noise ratio of 1500 can be obtained in the coding process. The large central peak in the middle of most interferograms

is very pronounced; in most cases, the amplitudes in the rest of the interferogram are considerably smaller. An 8-bit word is used to encode on a scale of plus and minus 128 levels, or a total of 256. One level is equal to the rms value of the noise. Larger amplitudes are divided by 10 electronically and then encoded. The position of the divide-by-10 circuit is indicated by a ninth bit. This effective dynamic compression maintains full accuracy for most points in the interferogram, but only one-tenth of the full accuracy for all points exceeding a tenth of the maximum possible amplitude. However, the one-tenth value in amplitude is exceeded for only a very small number of data points, compared to the total of 3408 points. The slightly reduced accuracy of a few data points can be shown to have negligible influence on the reproducibility of the spectra.

Thermal Design

Special design considerations are required to maintain an operating temperature of 250°K. The Nimbus spacecraft temperature is maintained at about 295°K by thermostat. In principle, it would be sufficient to cool only the detector, but to minimize the effect of stray radiation, it is advantageous to maintain a uniform temperature in the whole interferometer cube assembly. This requires good thermal conduction between all elements within the cube assembly while simultaneously isolating the assembly from the spacecraft and from all surfaces except one side which never faces the sun and the entrance aperture, of course. The exposed side will have a high emissivity beyond 5μ and will therefore radiate about $2 \cdot 10^{-2}$ watt cm^{-2} into outer space.

Considering a total radiating area of 12×25 cm^2, and allowing for small obscurations in the field-of-view, the total heat loss amounts to about 5 watts. The loss is compensated by the electrical power dissipated in the interferometer circuits located in the cube ($\sim$1 watt), by thermal energy conducted from the spacecraft through the mounting structure ($\sim$ 3 watts). The remaining difference of approximately 1 watt is generated by a small electrical heater which thermostatically controls the instrument to 250°K $\pm$ 2°K.

Image Motion Compensation

The interferometer is rigidly mounted to the spacecraft. Within the 11 seconds required for one interferogram, the orbital motion of Nimbus corresponds to about 80 km, or one-half the field-of-view. A change in radiance from the earth caused by the appearance or disappearance of clouds within the field-of-view would increase the difficulties of interpreting the spectra. The instrument registers some time-average of the spectra, but the spectral resolution is

also reduced. Sudden changes in the radiance at one wavelength will generate an amplitude modulation on the corresponding frequency in the interferogram. In the analysis, sidebands are generated which interfere with the signals from neighboring wavenumbers, thus reducing the overall accuracy as well as the spectral resolution.

The image-motion compensation effectively eliminates the smear and assures that the scenery does not change during the recording of one interferogram. This is accomplished by a slow rotation of the 45-degree calibration mirror. At the beginning of each interferogram, the mirror images an area 2 degrees ahead of the satellite subpoint into the interferometer. The same area is then kept under observation for 11 seconds. At the end of this period, the mirror points 2 degrees behind the satellite and advances to the starting position within the 5-second time interval between interferograms.

Auxiliary Measurements

A number of auxiliary measurements will be performed to facilitate better interpretation of the interferograms and to validate the operation of the instrument.

- Temperature Sensors

Various temperatures will be measured in the optical cube (the temperature of the bolometer mounting, the drive mirror, the beam splitter mounting, and a point near the entrance aperture) with an accuracy of 0.5°C. These temperature measurements will aid in the proper interpretation of the interferograms. The blackbody used for calibration purposes will be monitored by two bead thermistors to provide redundancy in this measurement.

- Voltage Measurements

A number of important voltages and execution commands will be monitored to certify proper operation of the instrument. The measured voltages include the bolometer bias voltage, the main power in the optical cube (-12 and -18 volts), and other strategically important voltages in the electronics compartment. A total of 15 auxiliary measurements will be performed.

DATA REDUCTION

The task of data reduction is more complicated for this experiment than for many others. A relatively high number of bits (almost 42,000 per interferogram) must be received, formatted, and presented to a digital computer for further processing and analysis. The purpose of this analysis program is to produce a power spectrum which is obtained from the Fourier transformation of the interferogram. This is necessary because the interferogram itself is not subject to detailed scientific analysis, and dependence upon the phases of the spectral components present is undesirable.

To test this analysis program, a synthesis program was created which simulates the performance of the instrument in detail, including the effects of obliquity of rays (caused by the finiteness of the optical solid angle), detector noise, and quantizing errors.

Various instrumentation design parameters were determined or confirmed with the aid of these synthesis and analysis computer programs. A description of the programs and some of the results of this study have been reported by Byrne (1965).

A sample, simulated interferogram is shown in Figure 5; Figures 6 to 9 show the transformed spectral profile for each of four cases. In every case the same source spectral profile was used (Wark, Alishouse and Yamamoto 1963, Atmosphere "G", Z_o = -6371); this is the spectrum for a clear warm atmosphere. This input spectrum is indicated on each spectral plot by the solid line segments shown, and the transformed spectrum is given by the "asterisked" line segments. Wherever noise was applied, the peak signal-to-noise (RMS) ratio was taken to be 1270:1, and except for Figure 9, each interferogram was computed for 3407 equally-spaced samples over a 10-second interval. The interferogram corresponding to the transformed spectrum of Figure 9 was taken for 1707 samples over the 10-second interval.

Figure 5 is the interferogram with all effects included, and Figure 6 is the corresponding transformed spectrum.

Figure 7 shows the effect on the transformed spectral profile of the finite solid angle and of quantization only; Figure 8, the effects of finite solid angle and detector noise only. Figure 9 includes all effects but, as noted above, the slower interferogram sampling rate was used.

In summary, results from the use of the two computer programs indicate that a sampling rate for IRIS of approximately four times the highest frequency

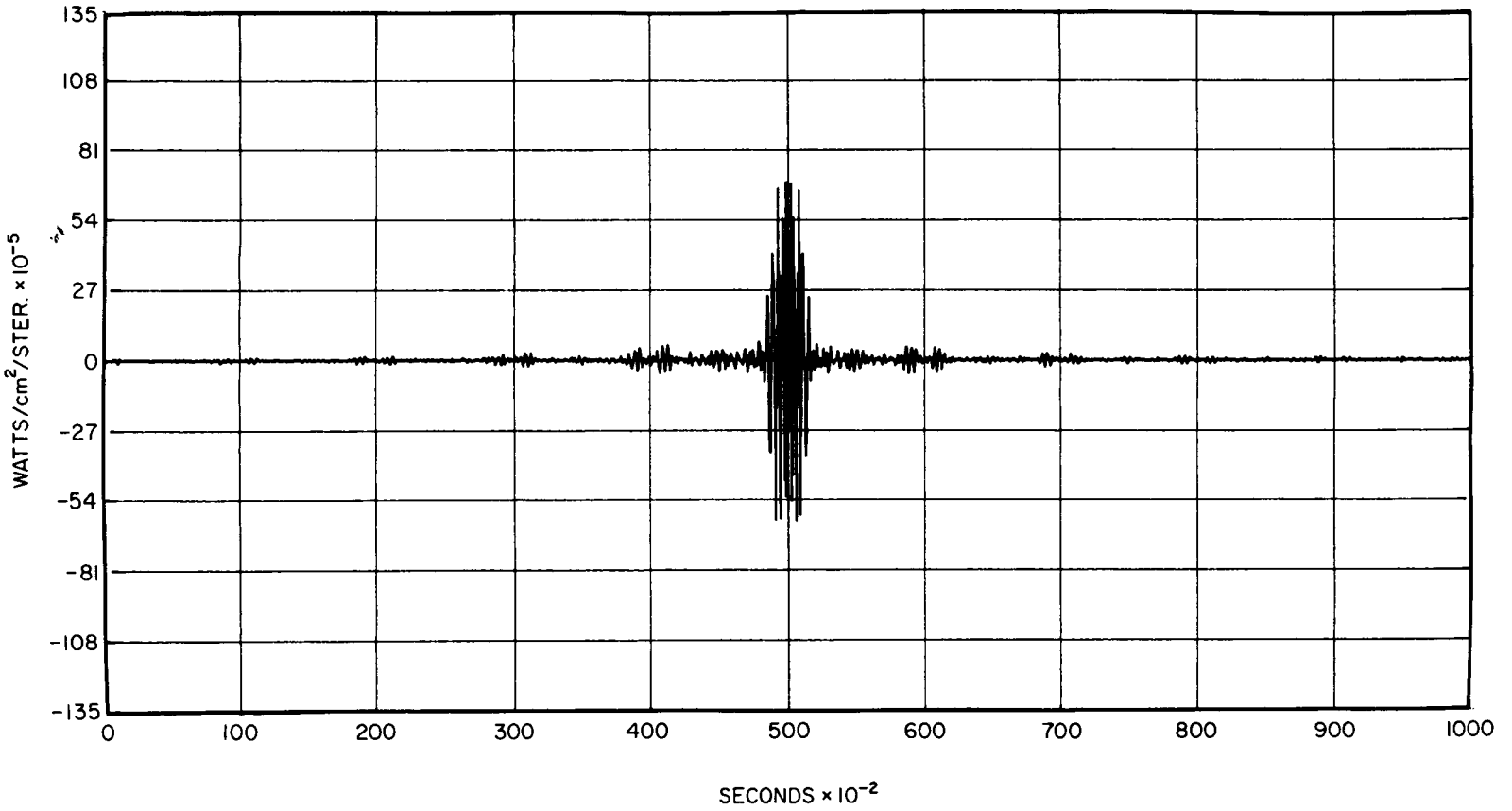

Response of the Interferometer to a Clear Warm Atmosphere was Calculated on a Digital Computer. Figure includes Effects of Finite Solid Angle, Detector, and Quantizing Noise

Figure 5–Simulated Interferogram

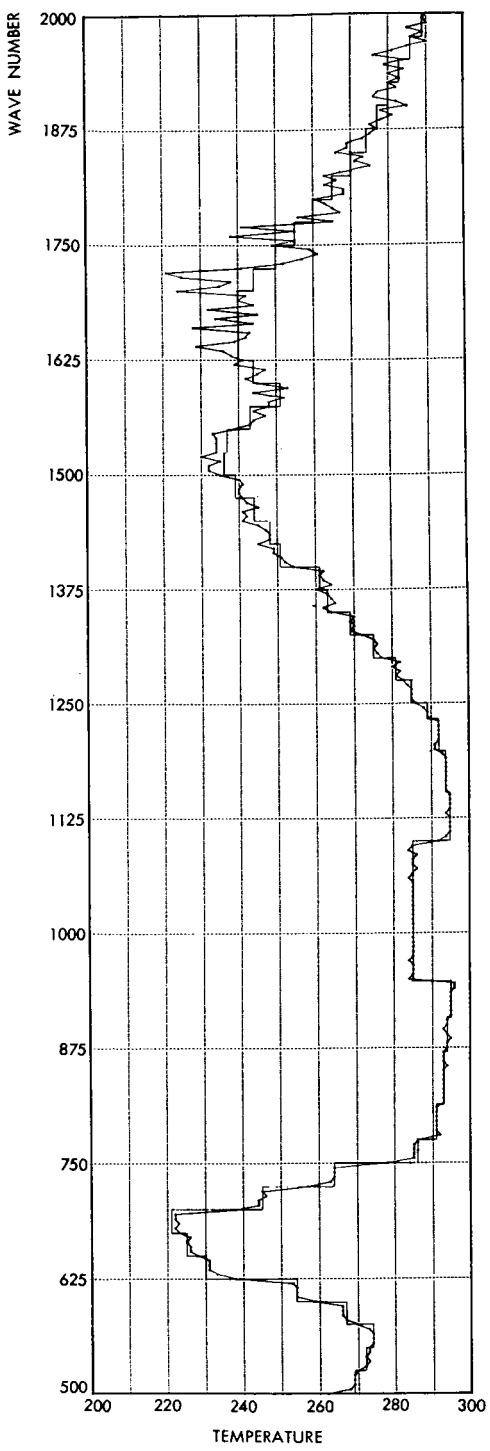

Figure 6–Power Spectrum Computed from Simulated Interferogram

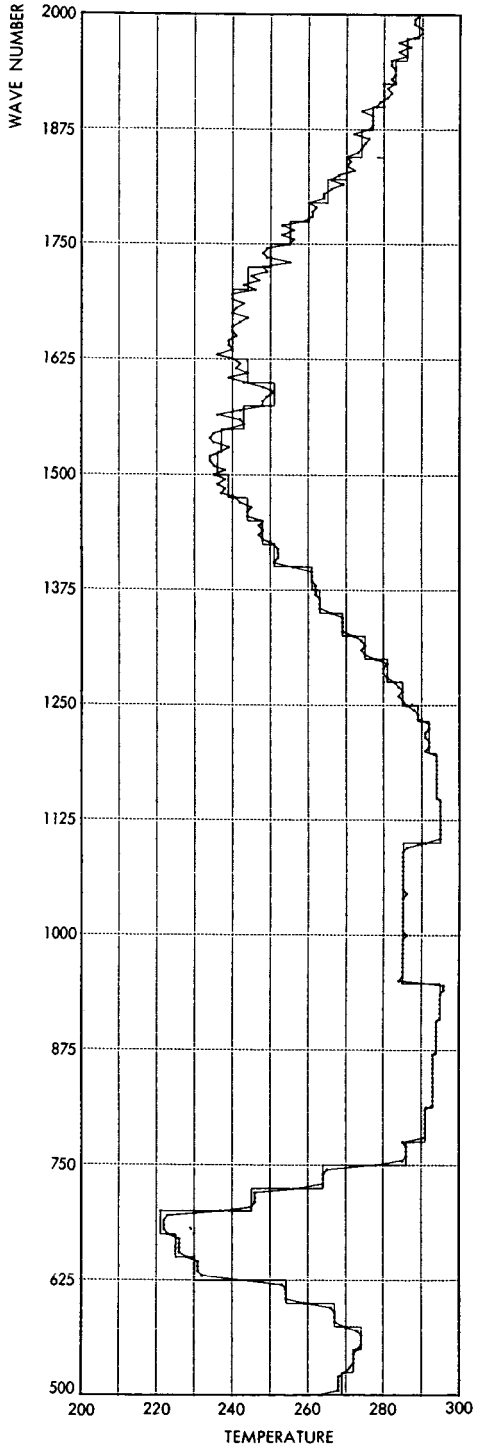

Figure 7 – Power Spectrum of Simulated Interferogram, Including Only the Effects of Finite Solid Angle and of Quantization

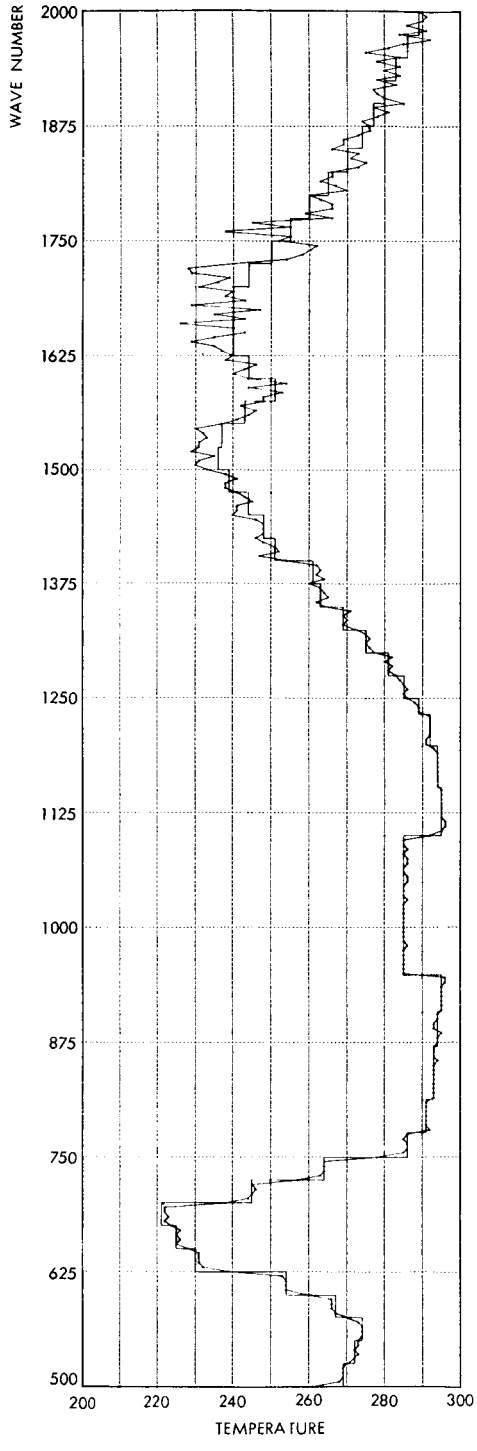

Figure 8 – Power Spectrum of Simulated Interferogram, Including Only the Effects of Finite Solid Angle and of Detector Noise

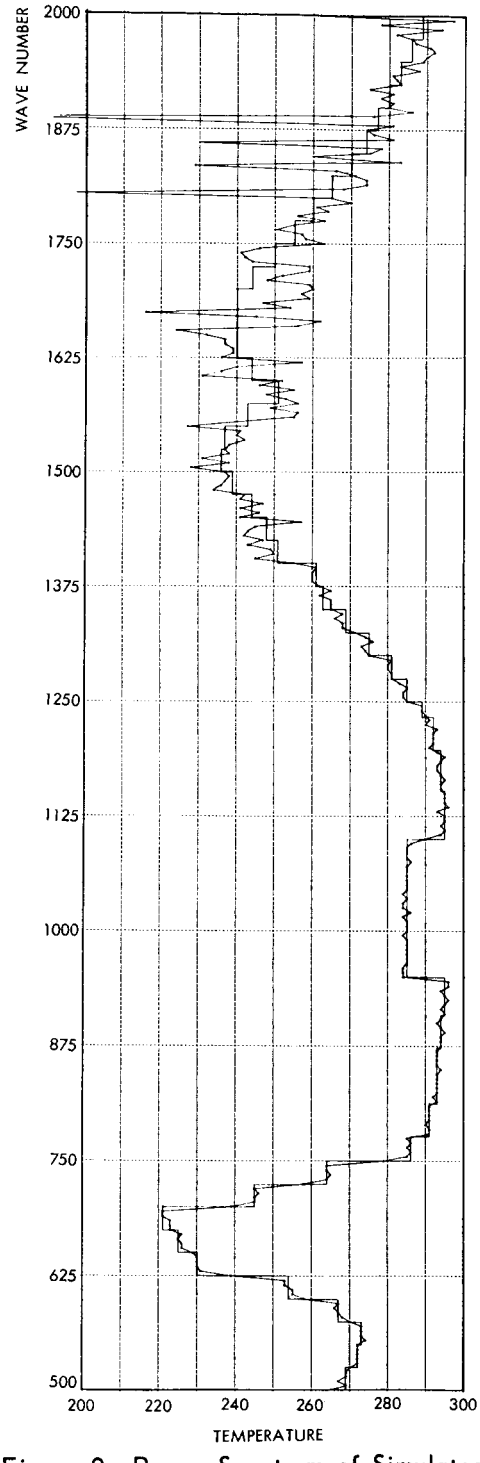

Figure 9 – Power Spectrum of Simulated Interferogram Derived from Only 1707 Samples

present is desirable. The effect of quantizing on the transformed spectral profile is, as anticipated, about the same as the effect of the mean expected signal-to-noise ratio at the detector. The gain switch, or the divide-by-ten, produces a negligible effect. The effect of the finite optical solid angle is less than that caused by digitization or noise at the detector.

DESIGN PARAMETERS FOR INFRARED INTERFEROMETER

Spectral range	2000-500 cm^{-1} (5 - 20μ) (possible extension to 300 cm^{-1} (33μ)
Spectral resolution	5 cm^{-1} over total range
Travel of drive mirror	0.2 cm
Diameter of effective aperture	3.6 cm
Detector	Thermistor bolometer in conical light pipe
Detector time constant	1 - 2 ms
Duration of interferogram	10.5 sec
Electrical frequencies at detector	20 - 80 cps
Sampling	Every second fringe of monochromatic source 5852.5 Å
Sampling rate	325 samples sec^{-1}
Samples per interferogram	3408
Housekeeping information	16 samples per interferogram (sampled 4 times)
Samples per frame	3472 samples
Bits per word	12
Bits per frame	41664
Interferograms per orbit	$\sim$ 420
Total number of bits per orbit	$18 \cdot 10^6$
Field of view	$1.57 \cdot 10^{-2}$ ster ($\sim 8°$)

In-flight calibration after every 14 interferograms

a. Outer space
b. 300°K blackbody

Monochromatic source	Neon lamps plus interference filter
Wavelength of reference source	5852.5 Å
Detector for reference source	Silicon junction
Frequency of reference signal	625 cps

REFERENCES

Byrne, L. H., 1965: Digital Computer Simulation of the Infrared Interferometer Spectrometer (IRIS) and Interferogram Analysis. Goddard Space Flight Center Report X-650-65-24.

Connes, J., Recherches sur la Spectroscopie par Transformation de Fourier. Rev. d'Opt., Vol. 40, pp. 45, 101, 157, 213 (1961).

Drayson, R. S., 1963: Errors in Atmospheric Temperature Structure Solutions from Remote Radiometric Measurements. Univ. of Michigan Tech. Rep., 25 pp.

Dreyfus, M. G., and Hillary, D., 1962: Satellite Infrared Spectrometer. Aerospace Engineering, Vol. 21, p. 42.

Fellgett, P., Spectrometric Interferential Multiples Power Measures Infra-Rouges sur les Etoiles, J. d'Physique et la Rad., Vol. 19, p. 237 (1958).

Fleming, H., Twomey, S., and Wark, D. Q., "The Inference of the Vertical Distribution of Atmospheric Parameters from Spectral Measurements," paper presented at the 25th national meeting of the Amer. Meteorol. Soc., Los Angeles (Jan. 1964).

Gebbie, H. A., J. Phys. Radium, Vol. 19, p. 230 (1959).

Goody, R. M., 1964: Atmospheric Radiation, I. Theoretical Basis, Oxford at the Clarendon Press, London.

Hanel, R. A., and Chaney, L., 1964: The Infrared Interferometer Spectrometer Experiment (IRIS). Vol. I, Martian Fly-by Mission, Goddard Space Flight Center Report X-650-64-204.

Jacquinot, P., Reports on Progress in Physics, Vol. 23, p. 263 (1960).

Kaplan, L. D., 1959: Inference of Atmospheric Structure from Remote Radiation Measurements. J. Opt. Soc. Amer., 49, pp. 1004-1007.

Kaplan, L. D., 1961: J. Quant. Spect. Radiative Transfer, Vol. 1, p. 98.

King, J. I. F., "Meteorological Inferences from Satellite Radiometry, I," J. Atmos. Sci., Vol. 20, p. 245 (1963).

King, J. I. F., 1956: The Radiative Heat Transfer of Planet Earth, in Scientific Uses of Earth Satellites, ed. by J. A. Van Allen, Univ. of Michigan Press, Ann Arbor, 316 pp.

King, J. I. F., 1964: Inversion by Slabs of Varying Thickness, J. Atmos. Sci., Vol. 21, p. 324.

Loewenstein, E. V., On the Correction of Phase Errors in Interferograms. App. Optics, Vol. 2, p. 491 (1963).

Lyon, R. J. P., Evaluation of Infrared Spectrophotometry for Compositional Analysis of Lunar and Planetary Soils. NASA Contract (NASA - 49/04) Quarterly Status Report No. 4, Stanford Research Institute (June 1963).

Mertz, L., J. Opt. Soc. Amer., Vol. 46, p. 548 (1956).

Mintz, Y., 1963: Meteorological Satellites and Numerical Weather Prediction. Rand Corp. Memorandum RM-3401-NASA.

Mintz, Y., 1964: Very Long Term Global Integration of the Primitive Equations of Atmospheric Motion. Proceedings WMO/IUGG Symposium on the Research and Development Aspects of Long Range Forecasting. Boulder, Colo.

Strong, J., and Vanesse, G. A., Interferometric Spectroscopy in the Far Infrared. J. Opt. Soc. Amer., Vol. 49, p. 844 (1959).

Wark, D. Q., "On Indirect Soundings of the Stratosphere from Satellites," J. Geophys. Res., Vol. 66, p. 77 (1961).

Wark, D. Q., Alishouse, J., and Yamamoto, G., 1963: Calculations of the Earth's Spectral Radiance for Large Zenith Angles. U. S. Weather Bureau Meteorological Satellite Laboratory Report No. 21.

Yamamoto, G., "Numerical Methods for Estimating the Stratospheric Temperature Distribution from Satellite Measurements in the CO_2 Band," J. of Meteorol., Vol. 18, p. 581 (1961).